The intracellular Ca^{2+} release channel TRPML1 regulates lower urinary tract smooth muscle contractility

Caoimhin S. Griffin[a], Michael G. Alvarado[a], Evan Yamasaki[a], Bernard T. Drumm[b,c], Vivek Krishnan[a], Sher Ali[a], Eleanor M. Nagle[a], Kenton M. Sanders[b], and Scott Earley[a,1]

[a]Department of Pharmacology, Center for Molecular and Cellular Signaling in the Cardiovascular System, Reno School of Medicine, University of Nevada, Reno, NV 89557-0318; [b]Department of Physiology and Cell Biology, Reno School of Medicine, University of Nevada, Reno, NV 89557-0318; and [c]Department of Life & Health Sciences, Dundalk Institute of Technology, Louth, Ireland A91 K584

Edited by Mark T. Nelson, University of Vermont, Burlington, VT, and approved October 13, 2020 (received for review August 12, 2020)

TRPML1 (transient receptor potential mucolipin 1) is a Ca^{2+}-permeable, nonselective cation channel that is predominantly localized to the membranes of late endosomes and lysosomes (LELs). Intracellular release of Ca^{2+} through TRPML1 is thought to be pivotal for maintenance of intravesicular acidic pH as well as the maturation, fusion, and trafficking of LELs. Interestingly, genetic ablation of TRPML1 in mice (*Mcoln1*$^{-/-}$) induces a hyperdistended/hypertrophic bladder phenotype. Here, we investigated this phenomenon further by exploring an unconventional role for TRPML1 channels in the regulation of Ca^{2+}-signaling activity and contractility in bladder and urethral smooth muscle cells (SMCs). Four-dimensional (4D) lattice light-sheet live-cell imaging showed that the majority of LELs in freshly isolated bladder SMCs were essentially immobile. Superresolution microscopy revealed distinct nanoscale colocalization of LEL-expressing TRPML1 channels with ryanodine type 2 receptors (RyR2) in bladder SMCs. Spontaneous intracellular release of Ca^{2+} from the sarcoplasmic reticulum (SR) through RyR2 generates localized elevations of Ca^{2+} ("Ca^{2+} sparks") that activate plasmalemmal large-conductance Ca^{2+}-activated K^+ (BK) channels, a critical negative feedback mechanism that regulates smooth muscle contractility. This mechanism was impaired in *Mcoln1*$^{-/-}$ mice, which showed diminished spontaneous Ca^{2+} sparks and BK channel activity in bladder and urethra SMCs. Additionally, ex vivo contractility experiments showed that loss of Ca^{2+} spark–BK channel signaling in *Mcoln1*$^{-/-}$ mice rendered both bladder and urethra smooth muscle hypercontractile. Voiding activity analyses revealed bladder overactivity in *Mcoln1*$^{-/-}$ mice. We conclude that TRPML1 is critically important for Ca^{2+} spark signaling, and thus regulation of contractility and function, in lower urinary tract SMCs.

calcium signaling | endolysosomes | ion channels | lower urinary tract | superresolution microscopy

The transient receptor potential (TRP) channel superfamily is a diverse group of ion channels that act through multiple signal transduction pathways to play a crucial role in sensory responses to light, smell, temperature, taste, and mechanical and painful chemical stimuli (1). TRP mucolipin (TRPML) is a subfamily of Ca^{2+}-permeable, nonselective cation channels that consists of three subtypes, TRPML1, TRPML2, and TRPML3, encoded by the genes *Mcoln1*, *Mcoln2*, and *Mcoln3*, respectively (2, 3). TRPML2 expression is primarily restricted to myeloid and lymphoid tissues (4, 5); TRPML3 is most plentiful in melanocytes and the cochlea (6), whereas TRPML1 channels exhibit a ubiquitous expression profile (7). The subcellular localization of TRPML is limited to the membranes of late endosomes and lysosomes (LELs), collectively known as endolysosomes. TRPML channel activity is dependent on the LEL membrane-specific phosphoinositide, phosphatidylinositol 3,5-bisphosphate (8), and is potentiated by LEL intraluminal acidity (6, 9). It has been shown that TRPML is functionally important in LEL maturation, trafficking, fusion, autophagy, and H^+ homeostasis (3, 10–13). Genetic deletion of TRPML1 in mice induces several gross abnormalities, including dense granulomembranous storage bodies in neurons, elevated plasma gastrin, vacuolization in the gastric mucosa, and retinal degeneration (14). Interestingly, however, an anatomical examination of these mice reveals dramatically distended bladders (14), leading us to question how TRPML1, an intracellular Ca^{2+}-release channel important in LEL function, affects bladder physiology.

The lower urinary tract (LUT) is composed of the urinary bladder and urethra—structures that serve the simple, reciprocal functions of storing and voiding urine (15). Coordinated contraction of bladder wall smooth muscle (BSM) and relaxation of both the proximal urethral smooth muscle (USM) and the striated external urethral sphincter allows for the voiding of urine. During the storage phase, BSM is in a relaxed state, whereas USM is tonically contracted to maintain continence (15, 16). While the bladder is filling, BSM exhibits nonvoiding contractions that have been demonstrated to drive afferent nerve activity to relay the feeling of bladder fullness to the central nervous system (CNS) (17). Similar nonvoiding contractions are also present in ex vivo BSM strip preparations, where they have been termed "spontaneous contractions" (18). Enhanced nonvoiding contractions, also known as detrusor overactivity (19), can lead to LUT symptoms such as feelings of increased urgency and greater frequency of urination, indicative of overactive bladder (OAB) syndrome (20).

Significance

TRPML1 (transient receptor potential mucolipin 1) is a Ca^{2+}-permeable, nonselective cation channel that is localized to late endosomes and lysosomes. Here, we investigated the function of TRPML1 channels in regulating lower urinary tract (LUT) smooth muscle cell (SMC) contractility. We found that TRPML1 forms a stable signaling complex with ryanodine receptors (RyRs) in the sarcoplasmic reticulum (SR). We further showed that TRPML1 channels are important for initiating an essential Ca^{2+}-signaling negative feedback mechanism between RyRs on SR membranes and K^+ channels on the plasma membrane. Knockout of TRPML1 channels in mice impaired this pathway, resulting in LUT smooth muscle hypercontractility and symptoms of overactive bladder. Our findings demonstrate a critical role for TRPML1 in LUT function.

Author contributions: C.S.G., K.M.S., and S.E. designed research; C.S.G., M.G.A., E.Y., B.T.D., V.K., S.A., and E.M.N. performed research; C.S.G., M.G.A., E.Y., and S.E. analyzed data; and C.S.G. and S.E. wrote the paper.

This article is a PNAS Direct Submission.

See online for related content such as Commentaries.

[1]To whom correspondence may be addressed. Email: searley@med.unr.edu.

This article contains supporting information online at https://www.pnas.org/lookup/suppl/doi:10.1073/pnas.2016959117/-/DCSupplemental.

First published November 16, 2020.

Spontaneous contractions of BSM are directly correlated with bursts of action potentials and are reliant on voltage-dependent $Ca_V1.2$ channel (VDCC)-mediated global increases in cytosolic $[Ca^{2+}]$ in bladder smooth muscle cells (BSMCs) (21–23). In contrast, transient subcellular increases in cytosolic $[Ca^{2+}]$, known as "Ca^{2+} sparks," play an opposing role in regulating BSMC contractility. Ca^{2+} sparks are rapid, large-amplitude, highly localized, spontaneous Ca^{2+} signals that originate from clusters of ryanodine type 2 receptors (RyR2s) located on the sarcoplasmic reticulum (SR) of SMCs (24). In BSMCs, RyR2s are functionally coupled to plasmalemmal Ca^{2+}-activated large-conductance K^+ (BK) channels, such that a single Ca^{2+} spark can activate up to 100 BK channels, giving rise to large-amplitude outward currents known as spontaneous transient outward currents (STOCS) that lead to membrane potential hyperpolarization and SMC relaxation (25–28). Inhibition of RyR2s or BK channels has a profound hypercontractile effect on spontaneous contractions of BSM (reviewed in ref. 29), identifying the Ca^{2+} spark–BK channel signaling cascade as a pivotal regulator of BSMC resting membrane potential, excitability, and contractility. In BSMCs, the steepness of the gradient between LEL intraluminal $[Ca^{2+}]$ (~0.5 mM) (30) and the surrounding cytosol (100 nM) prompted us to investigate the unconventional hypothesis that opening of Ca^{2+}-permeable TRPML1 channels on the membrane of LELs could stimulate or potentiate RyR2 activity through Ca^{2+}-induced Ca^{2+} release, and thereby regulate Ca^{2+} spark–BK channel signaling and BSM contractility. Urethral smooth muscle cells (USMCs) also exhibit functional BK channel currents that are activated by RyR-mediated Ca^{2+} release (31). Therefore, TRPML1 channels could also influence RyR–BK channel signaling in USMCs.

In the current study, we confirmed that global TRPML1-knockout mice (*Mcoln1*$^{-/-}$) display a hyperdistended/hypertrophic bladder phenotype. We further found that, among transcripts of TRPML subtypes, those for TRPML1 were the most abundantly expressed in sorted BSMCs (enriched by fluorescence-activated cell sorting [FACS]) enzymatically dispersed from the bladder. Four-dimensional (4D) lattice light-sheet live-cell imaging, used to track LEL mobility, and superresolution microscopy established that LEL-localized TRPML1 channels and RyR2s formed stable signaling complexes in native BSMCs. Ca^{2+} sparks and their associated BK channel-mediated STOCs were virtually absent in BSMCs and significantly impaired in USMCs isolated from *Mcoln1*$^{-/-}$ mice. Ex vivo contractility experiments showed that BSM strip spontaneous contractions and cholinergic-induced contractions were significantly enhanced in *Mcoln1*$^{-/-}$ mice, as were α_1-adrenergic receptor (α_1-AR)-mediated contractions of proximal USM. An analysis of in vivo voiding activity demonstrated a marked increase in voiding frequency in *Mcoln1*$^{-/-}$ mice indicative of OAB. We conclude that, under physiological conditions, TRPML1 channels regulate the Ca^{2+} spark–BK channel signaling pathway, thereby maintaining normal LUT smooth muscle function.

Results

TRPML Channel Expression in BSMCs. An examination of the abdominal cavity of global *Mcoln1*$^{-/-}$ mice following killing revealed a grossly distended bladder compared with that of wild-type (WT) littermates (Fig. 1 *A* and *B*), a phenotype also noted by Venugopal et al. (14). Examination of whole bladders emptied of urine revealed that bladders from *Mcoln1*$^{-/-}$ mice were significantly heavier than those from WT mice (Fig. 1*C*), indicative of bladder hypertrophy in *Mcoln1*$^{-/-}$ mice. TRPML1 knockout in *Mcoln1*$^{-/-}$ mice was verified using droplet digital PCR (ddPCR) and the Wes automated capillary protein-detection system. A transcriptional analysis of TRPML channel subtypes (*Mcoln1*, *-2*, and *-3*) showed high levels of *Mcoln1* mRNA expression in WT whole BSM strips, whereas *Mcoln2* and *-3* were expressed at much lower levels (Fig. 1*D*). We further found that *Mcoln1* transcripts were undetectable in *Mcoln1*$^{-/-}$ mice and that expression levels of *Mcoln3* were unchanged in these mice. A small, but statistically significant, increase in *Mcoln2* mRNA was observed in *Mcoln1*$^{-/-}$ mice compared with WT mice (Fig. 1*D*). An analysis of TRPML1 expression at the protein level identified a single band at the expected molecular weight (~60 kDa) in WT BSM strips that was not present in muscle strips from *Mcoln1*$^{-/-}$ mice (Fig. 1*E*). Homogeneous populations of native BSMCs were obtained from bladders isolated from smMHC$^{Cre/eGFP}$ reporter mice and subsequently purified and concentrated using FACS. Using qRT-PCR, sorted BSMCs showed undetectable levels of mRNA encoding *Pdgfra* (interstitial cell marker), *Ptprc* (leukocyte marker), and *Uchl1* (neuronal cell marker); however, transcripts for the SMC marker, *Myh11*, were enriched compared with samples of unsorted cells (*SI Appendix*, Fig. S1). Further transcriptional analyses showed that *Mcoln1* was highly expressed in sorted BSMCs, whereas *Mcoln2* and *Mcoln3* were present at much lower levels in these samples (Fig. 1*F*). We conclude that TRPML1 is highly expressed in BSMCs relative to TRPML2 and TRPML3 subtypes, and that genetic deletion of *Mcoln1* induces a hyperdistended and hypertrophic bladder phenotype, an indication of the channel's functional relevance in the bladder.

Endolysosomes Are Immobile in BSMCs. It is widely reported that TRPML1 channels contribute to the intracellular trafficking of LELs (reviewed in ref. 3). In this study we investigated the mobility of these intracellular organelles in freshly isolated BSMCs using an LEL-specific fluorescent dye (LysoTracker Red) (32). Freshly isolated BSMCs were labeled with LysoTracker (Fig. 2*A*) and imaged for 10 min using 4D lattice light-sheet live-cell microscopy (33). The mobility of LysoTracker-labeled structures was analyzed using single particle tracking. Surprisingly, we found that the majority of LELs in freshly isolated BSMCs were effectively motionless (Movie S1). Post hoc particle analysis revealed that on average LELs in BSMCs moved less than 0.4 μm over the entire recording period (Fig. 2 *B*, *C*, *G*, and *H*). As a comparison, we investigated the mobility of LELs in primary, unpassaged, proliferative BSMCs derived from the same mice that had been used for the freshly isolated cell studies, but cultured in the presence of serum for 6 d. Interestingly, LysoTracker-labeled LELs were highly mobile in proliferative BSMCs in comparison to those in freshly isolated BSMCs (Fig. 2*D* and Movie S2), moving on average 2.4 μm over the recording period. LELs demonstrated slow, Brownian-type diffusion, as well as quick, linear, long-range movements (Fig. 2 *E–H* and Movie S2). Notably, we found that proliferative BSMCs possessed a larger cell-wide density of LELs compared to freshly isolated BSMCs (Fig. 2*I*). These data suggest that in mature freshly isolated BSMCs, LELs are essentially immobile, and that a return to a proliferative phenotype considerably increases the mobility of these intracellular organelles.

Nanoscale Localization of TRPML1-Positive LELs to RyR2 Clusters in Native BSMCs. The stark contrast in LEL mobility between freshly isolated BSMCs and cultured proliferative BSMCs suggested the possibility that stationary LELs could form stable signaling complexes in freshly isolated BSMCs. To investigate this hypothesis, we utilized immunofluorescence labeling in conjunction with ground state depletion followed by individual molecule return (GSDIM) superresolution microscopy (34–36) in native BSMCs to examine the subcellular nanoscale colocalization of TRPML1 channel clusters with RyR2s and the LEL membrane-bound protein, Lamp-1 (lysosomal-associated membrane protein 1). Using DNA origami-based nanorulers, we have previously shown that the lateral resolution of our GSDIM system is 20 to 40 nm (37–39).

First, we tested the relative specificity of our anti-TRPML1 antibody and our detecting fluorescent secondary antibodies. In a previous study, we used superresolution microscopy to demonstrate that cerebral artery SMCs isolated from *Mcoln1*$^{-/-}$ mice, unlike those from WT mice, lacked immunoreactivity to

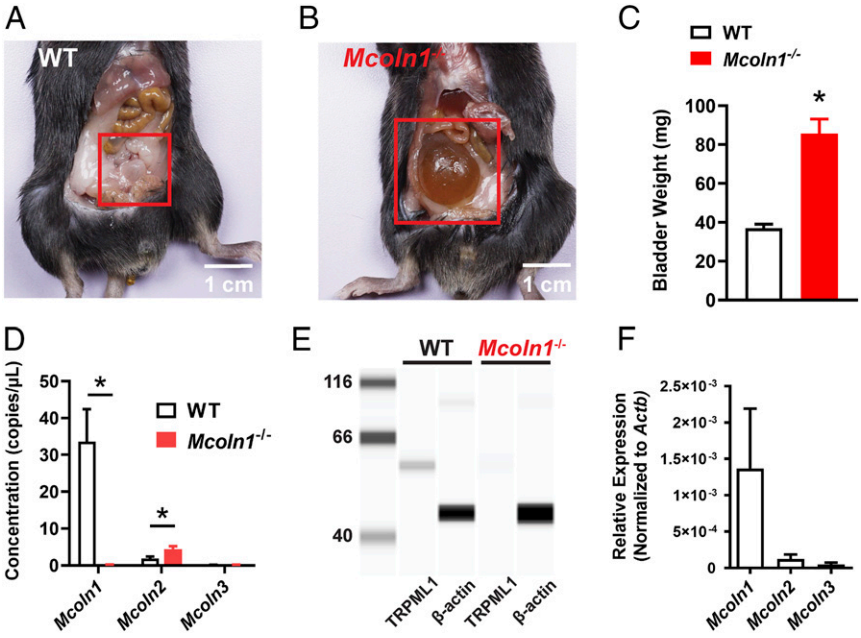

Fig. 1. Bladder abnormalities in *Mcoln1*$^{-/-}$ mice and TRPML subtype expression in *Mcoln1*$^{-/-}$ BSMCs. (*A* and *B*) Representative images of the typical bladder anatomy observed in WT mice (*A*) and the hyperdistended/hypertrophic bladder phenotype observed in all *Mcoln1*$^{-/-}$ mice (*B*). (*C*) Summary data illustrating the differences in whole-bladder weight (in milligrams) between WT and *Mcoln1*$^{-/-}$ mice ($n = 8$ animals/group; *$P < 0.05$). (*D*) ddPCR analysis of the expression of *Mcoln1*, *Mcoln2*, and *Mcoln3* mRNA (copies/μL PCR) in BSM from WT and *Mcoln1*$^{-/-}$ mice ($n = 4$ animals/group; *$P < 0.05$). (*E*) Representative Wes analysis results for TRPML1 protein in BSM. A single band (~60 kDa) was detected in lysates of BSM from WT mice, but was absent in lysates of BSM from *Mcoln1*$^{-/-}$ mice ($n = 4$ animals/group). β-Actin was used as a loading control. (*F*) qRT-PCR analysis of *Mcoln1*, *Mcoln2*, and *Mcoln3* mRNA expression levels (normalized to *Actb*) in FACS-enriched homogeneous populations of BSMCs ($n = 3$ animals/group). All data are presented as means ± SEM.

our anti-TRPML1 antibody (39). In the current study, we validated the specificity of our anti-TRPML1 antibody using the Wes protein-detection system (Fig. 1*E*). We also tested the specificity of our anti-RyR2, anti-Lamp-1, and anti-TRPML1 antibodies by comparing the immunoreactivity and labeling density of these antibodies in isolated BSMCs incubated with primary and corresponding secondary antibodies with those in cells incubated with secondary antibodies alone (*SI Appendix*, Fig. S2).

Isolated native BSMCs were colabeled for TRPML1 and Lamp-1, RyR2 and Lamp-1, or TRPML1 and RyR2 proteins. Subsequent imaging using GSDIM in epifluorescence illumination mode and analysis of data revealed that the targeted proteins were not homogeneously distributed throughout the cell, but instead were present as defined protein clusters (Fig. 3 *A*–*C*). Postacquisition image analyses revealed that TRPML1 and RyR2 cluster sizes were exponentially distributed (Fig. 3 *D* and *E*); however, the density of RyR2 clusters (clusters/μm^2) was approximately twofold higher than that of TRPML1 clusters (Fig. 3*F*). RyR2 and TRPML1 clusters exhibited a broader cellular distribution in comparison to Lamp-1 (Fig. 3 *A*–*C*). Lamp-1 clusters aggregated into large ovoid-like structures resembling LELs that were between 62,000 and 1,000,000 nm^2 in size (Fig. 3*G*)—values that are consistent with the sizes of LELs reported in a prior study (40). Using object-based analysis, we found that Lamp-1–immunolabeled LELs colocalized with a significant number of TRPML1 protein clusters, such that most of the LELs were TRPML1-positive (75.3%; 70 of 93).

The distance between RyR2 protein clusters and Lamp-1–labeled LELs could provide an indication of whether TRPML1 channels were within sufficient proximity to influence RyR2 activity. Therefore, using nearest-neighbor analysis of our acquired images (Fig. 3*B*), we measured the distance between individual RyR2 clusters and the nearest outer edge of Lamp-1–labeled LELs. A distribution plot of our data revealed that a significant number of RyR2 clusters were located within 0 to 40 nm of a Lamp-1–positive LEL (Fig. 3*H*), and showed that RyR2 clusters at a distance of 50 to 500 nm from LELs were distributed randomly. Additionally, further analysis of RyR2 and TRPML1 colabeled cells revealed colocalization of a significantly greater number of TRPML1–RyR2 clusters compared with a simulated random distribution (Fig. 3*I*). Colocalization was determined as the geometric center of a protein cluster occupying that same two-dimensional (2D) space as protein clusters in the opposing wavelength. Taken together, our data suggest that a substantial fraction of Lamp-1–localized TRPML1 channels are situated within 40 nm of RyR2 clusters in freshly isolated BSMCs, further supporting our concept that TRPML1 channels in native BSMCs localize to stationary LELs, where they form stable signaling complexes with RyR2s.

BSMCs from *Mcoln1*$^{-/-}$ Mice Display Impaired Spontaneous Ca^{2+} Sparks and BK Channel Activity Leading to Smooth Muscle Hypercontractility. The Ca^{2+} spark–BK channel signaling complex is a pivotal regulator of BSMC resting membrane potential, excitability, and contractility (29). To determine the functional contribution of TRPML1 channels to this pathway, we next investigated Ca^{2+} spark activity in freshly isolated BSMCs from WT and *Mcoln1*$^{-/-}$ mice. Using spinning-disk confocal microscopy with a Ca^{2+}-sensitive fluorophore (Fluo-4 AM), we observed spontaneous Ca^{2+} sparks in nearly all BSMCs (18/20) isolated from WT mice (Fig. 4*A* and Movie S3). However, spontaneous Ca^{2+} sparks were not detected in almost all of the BSMCs (2/20) isolated from *Mcoln1*$^{-/-}$ mice (Fig. 4*B* and Movie S4). Specifically, we found that the number of Ca^{2+} spark sites per cell and the frequency of Ca^{2+} spark events (Fig. 4 *C* and *D*) was greatly diminished in BSMCs from *Mcoln1*$^{-/-}$ mice compared to those of WT mice. To determine if the effects of *Mcoln1*$^{-/-}$ knockout on Ca^{2+} spark activity is brought about by alterations in total SR [Ca^{2+}], we applied bolus applications of caffeine (10 mM) to BSMCs from both WT and *Mcoln1*$^{-/-}$ mice. Caffeine-evoked global increases in

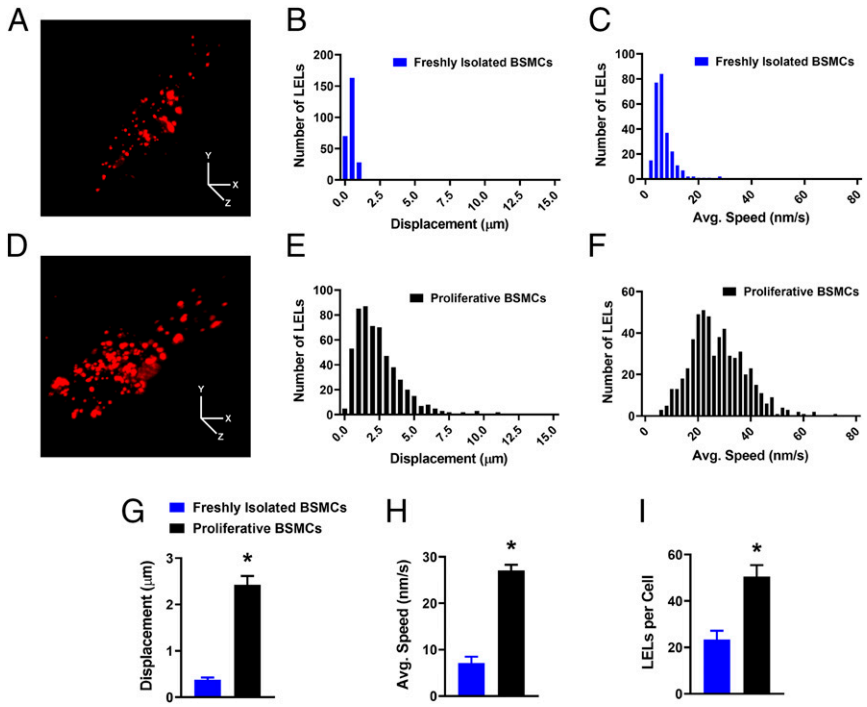

Fig. 2. LELs are immobile in freshly isolated BSMCs. (*A*) Representative lattice light-sheet image of a freshly isolated BSMC stained with LysoTracker Red. (Scale bars, 10 μm.) (*B* and *C*) Histogram showing the distributions of LEL total displacement (*B*) and average speed (*C*) within freshly isolated BSMCs, recorded over a 10-min period. A total of 262 LELs (n = 12 cells) were tracked and analyzed. (*D*) Representative lattice light-sheet image of a cultured, proliferative BSMC stained with LysoTracker Red. (Scale bars, 10 μm.) (*E* and *F*) Histogram showing the distributions of LEL total displacement (*E*) and average speed (*F*) within proliferative BSMCs, recorded over a 10-min period. A total of 555 LELs (n = 11 cells) were tracked and analyzed. Summary data showing the mean values for LEL (*G*) displacement and (*H*) average speed, and the (*I*) cellular density of LELs in both freshly isolated and proliferative BSMCs (freshly isolated BSMCs, n = 12 cells from n = 4 mice; proliferative BSMCs, n = 11 cells from n = 4 mice; $^*P < 0.05$). All data are shown as mean ± SEM.

BSMC cytosolic [Ca^{2+}] did not differ between WT and *Mcoln1*$^{-/-}$ mice (Fig. 4*E*), indicative that the lack of spontaneous Ca^{2+} spark activity in BSMCs from *Mcoln1*$^{-/-}$ mice is not due to significant differences in SR [Ca^{2+}].

Activation of BK channels by RyR2-mediated Ca^{2+} sparks generates large-amplitude STOCs in urinary bladder SMCs. Since spontaneous Ca^{2+} spark activity was essentially absent in BSMCs from *Mcoln1*$^{-/-}$ mice, we next investigated and compared STOC activity in freshly isolated BSMCs from WT and *Mcoln1*$^{-/-}$ mice by patch-clamp electrophysiology using the perforated-patch configuration. BSMCs from WT mice, voltage clamped at physiologically realistic membrane potentials (~40 mV), exhibited robust STOC activity, whereas STOCs in BSMCs isolated from *Mcoln1*$^{-/-}$ mice were nearly undetectable (Fig. 5*A*). The frequencies and amplitudes of STOCs were significantly reduced over a range of membrane potentials (−60 to −20 mV) in BSMCs isolated from *Mcoln1*$^{-/-}$ mice (Fig. 5 *B* and *C*). Whole-cell BK currents were recorded from BSMCs isolated from WT and *Mcoln1*$^{-/-}$ mice to determine whether reduced plasmalemmal BK channel expression or altered BK channel function was responsible for the observed reduction in STOCs. The BK-sensitive component of the current was isolated by evoking whole-cell K^+ currents with voltage steps in the presence of the BK channel antagonist paxilline (1 μM) (*SI Appendix*, Fig. S3*A*). These experiments revealed no difference in BK current density (pA/pF) between BSMCs isolated from WT and *Mcoln1*$^{-/-}$ mice (*SI Appendix*, Fig. S3*B*). Evaluation of the transcriptional expression of *Ryr2* (encoding RyR2), *Kcnma1* (encoding the BKα pore-forming subunit), and *Kcnmb1* (encoding the BKβ1 regulatory subunit) using ddPCR showed no significant differences in BSM from WT and *Mcoln1*$^{-/-}$ mice (*SI Appendix*, Fig. S3*C*). Taken together, these data suggest that genetic deletion of TRPML1 impairs the generation of Ca^{2+} sparks and their associated STOCs in BSMCs and indicate that the reduction in Ca^{2+} spark–BK channel signaling in *Mcoln1*$^{-/-}$ mice is not due to altered expression of unique and vital components of the RyR2–BK channel pathway.

To further investigate the impact of *Mcoln1* deletion on STOCs, a pharmacological approach was used. Selective blockers of TRPML1 activity are not available commercially. However, the selective TRPML1 agonist, ML-SA1 (41), increased STOC frequency significantly in BSMCs isolated from WT mice. Effects of ML-SA1 on STOCs were not detected in BSMCs from *Mcoln1*$^{-/-}$ mice (holding potential of −30 mV; Fig. 5 *D* and *E*). Collectively, genetic and pharmacological manipulations of STOC activity indicate that TRPML1 channel activity is essential for the spontaneous activity of the Ca^{2+} spark–BK channel signaling cascade in BSMCs.

The regulation of BSM contractility by TRPML1 channels was assessed using ex vivo isometric tension experiments. These experiments showed that spontaneous contractions of BSM strips from *Mcoln1*$^{-/-}$ mice were hypercontractile relative to WT mice (Fig. 6*A*). Specifically, we found that the average contraction amplitude was significantly greater in BSM strips from *Mcoln1*$^{-/-}$ mice, but the contraction frequency was reduced (Fig. 6 *B* and *C*). Voiding contractions of the bladder are predominantly mediated by cholinergic activation of postjunctional muscarinic type 3 receptors (M_3Rs) (42). We found that BSM strips from *Mcoln1*$^{-/-}$ mice displayed an increased contractile response and enhanced sensitivity to stimulation with the nonselective muscarinic receptor agonist carbachol (CCh) (Fig. 6 *D* and *E*) compared with strips from WT mice. No difference in M_3R (*Chrm3*) transcripts (*SI Appendix*, Fig. S3*C*) or proteins (*SI Appendix*, Fig. S4) were resolved in BSM isolated from WT and

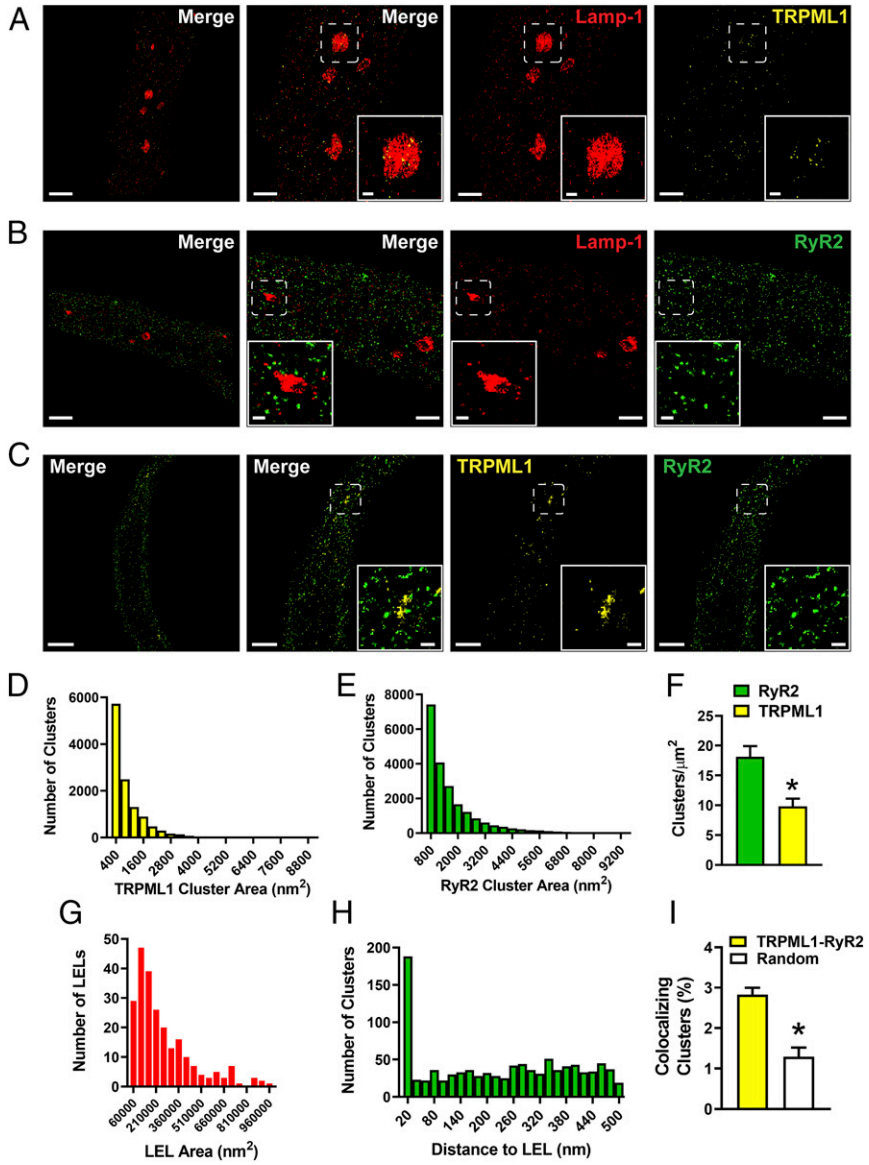

Fig. 3. Nanoscale colocalization of TRPML1 with RyR2 and Lamp-1 in native BSMCs. (*A*–*C*) Representative superresolution localization maps of isolated BSMCs coimmunolabeled for Lamp-1 and TRPML1 (*A*), Lamp-1 and RyR2 (*B*), or TRPML1 and RyR2 (*C*). (Scale bars, 2 μm.) Representative of $n = 8$ to 10 cells isolated from $n = 3$ to 4 animals. The second panel shows a magnified view of the region enclosed in the white boxes. (Scale bars, 1 μm.) *Insets* show magnified views of the indicated regions of interest. (Scale bars, 0.2 μm.) (*D* and *E*) Histograms showing the distribution of the surface areas of individual protein clusters for TRPML1 (*D*) and RyR2 (*E*) (TRPML1, $n = 11{,}862$ clusters; RyR2, $n = 21{,}030$ clusters). (*F*) TRPML1 and RyR2 protein cluster density ($n = 12$ cells, $n = 4$ animals per group; $^*P < 0.05$). (*G*) Histogram showing that individual Lamp-1 ovoid metastructures are between 62,000 and 1,000,000 nm^2 in size (mean area = 270,779 ± 13,888 nm^2, $n = 240$). (*H*) Nearest-neighbor analysis showing the distribution of distances between the center of RyR2 protein clusters and the outer edge of Lamp-1–positive LELs ($n =$ 1,019 RyR2 protein clusters). (*I*) Object-based analysis comparing the fraction of TRPML1 and RyR2 colocalizing clusters with a simulated random distribution of clusters (TRPML1–RyR2, 2.83% ± 0.17%; random, 1.29% ± 0.23%; $n = 8$ cells from three animals; $^*P < 0.05$). All data are presented as means ± SEM.

Mcoln1$^{-/-}$ mice, suggesting that the observed enhancement in M_3R-mediated contractions was not due to increased receptor expression. BSM contractions induced by high extracellular K^+ (60 mM) did not differ between WT mice and *Mcoln1*$^{-/-}$ mice (*SI Appendix*, Fig. S5*A*), indicating that BSM hypercontractility is most likely unrelated to altered VDCC function or other pathways regulating contractility.

Urethral Smooth Muscle from *Mcoln1*$^{-/-}$ Mice Is Hypercontractile. The RyR2–BK channel axis has been shown to regulate USM contractility (31, 43). However, spontaneous Ca^{2+} spark activity has never been optically detected or reported in USMCs, though STOCs have been observed in these cells (31). Therefore, we next sought to detect the presence of Ca^{2+} sparks in USMCs and investigate the role of TRPML1 channels in regulating the Ca^{2+} spark–BK channel pathway in USM. Using spinning-disk confocal microscopy, we detected significant spontaneous Ca^{2+} spark activity in freshly isolated USMCs (Fig. 7*A* and Movie S5). We found that nearly all (17/19) of the USMCs isolated from WT mice exhibited spontaneous Ca^{2+} spark activity (Fig. 7*A*), but were detected in only ∼45% of USMCs obtained from *Mcoln1*$^{-/-}$ mice (Fig. 7*B* and Movie S6). Further, the number of Ca^{2+} spark sites per cell and the mean frequency of Ca^{2+} sparks were considerably lower in USMCs from *Mcoln1*$^{-/-}$ mice compared with controls (Fig. 7 *C* and *D*). Using caffeine-evoked global increases in USMC [Ca^{2+}] (Fig. 7*E*), we also demonstrate that the impaired spontaneous Ca^{2+} activity in USMCs from *Mcoln1*$^{-/-}$ mice is not due to

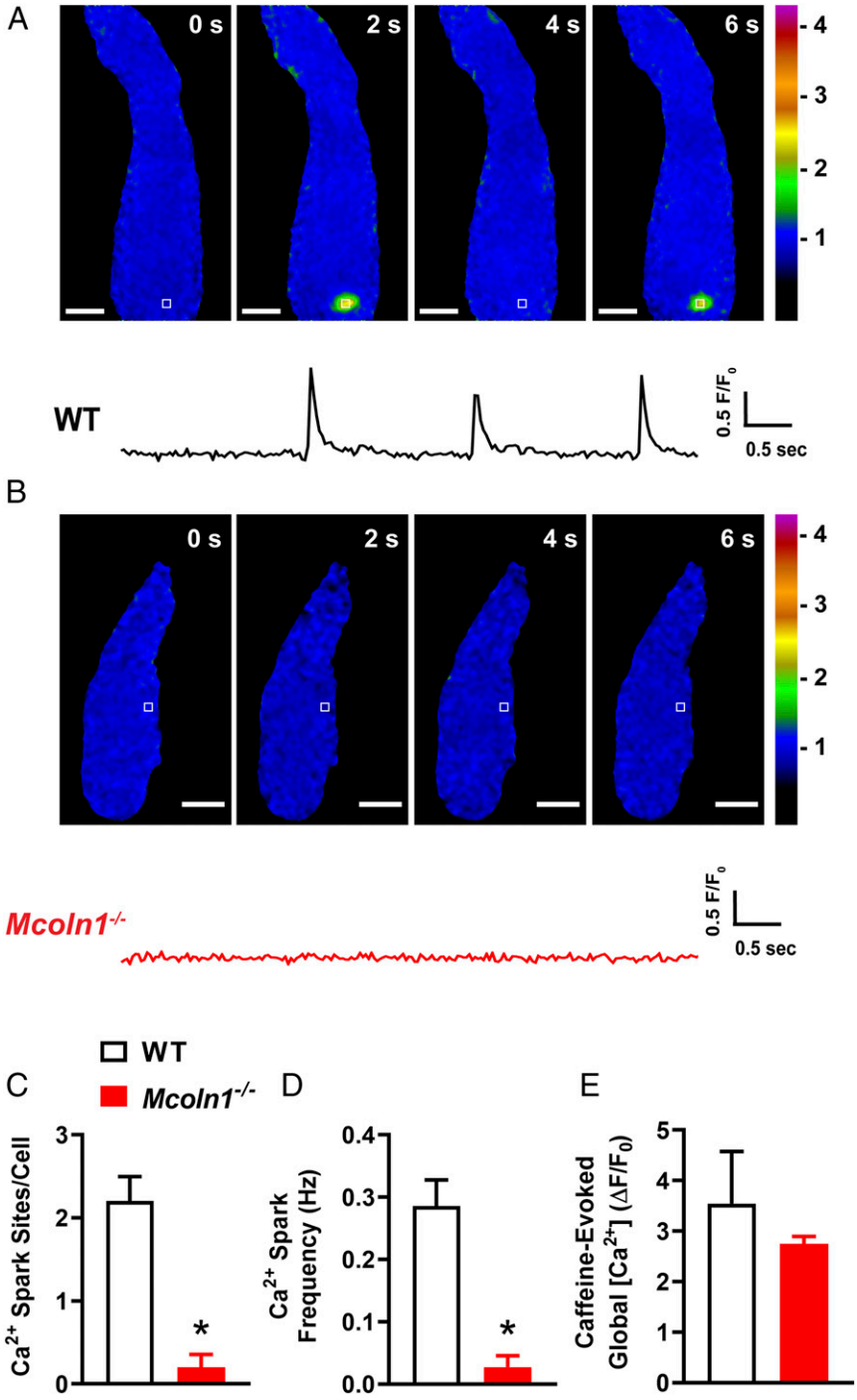

Fig. 4. BSMCs from *Mcoln1*$^{-/-}$ mice lack spontaneous Ca^{2+} sparks. (*A*) Representative confocal time course images of a Ca^{2+} spark site (in seconds) in a Fluo-4 AM loaded BSMC from a WT mouse, and trace showing changes in fractional fluorescence (F/F_0) in a defined region of interest (white box). (Scale bar, 10 μm.) (*B*) Representative confocal time course images (in seconds) and complimentary trace recorded from a BSMC isolated from a *Mcoln1*$^{-/-}$ mouse showing lack of Ca^{2+} spark activity. (Scale bar, 10 μm.) (*C* and *D*) Summary data showing (*C*) the number of spontaneous Ca^{2+} spark sites per cell and (*D*) Ca^{2+} spark frequency in BSMCs isolated from WT and *Mcoln1*$^{-/-}$ mice (WT, $n = 20$ cells from $n = 4$ mice; *Mcoln1*$^{-/-}$, $n = 20$ cells from $n = 4$ mice; $^*P < 0.05$). (*E*) Total SR Ca^{2+} store load in BSMCs from WT and *Mcoln1*$^{-/-}$ mice, assessed by imaging changes in global intracellular [Ca^{2+}] in response to administration of caffeine (10 mM) (WT, $n = 7$ cells from $n = 4$ mice; *Mcoln1*$^{-/-}$, $n = 7$ cells from $n = 4$ mice). All data are presented as means ± SEM.

differences in SR [Ca^{2+}]. We also pharmacologically characterized the Ca^{2+} spark activity in USMCs isolated from WT mice using the RyR inhibitor ryanodine. We found that ryanodine (10 μM) essentially abolished Ca^{2+} spark activity (*SI Appendix*, Fig. S6), indicating that these events are mediated by RyRs in USMCs.

We also investigated STOC activity electrophysiologically in freshly isolated USMCs from WT and *Mcoln1*$^{-/-}$ mice using the perforated-patch configuration of the patch-clamp technique. USMCs isolated from WT mice displayed STOCs at membrane potentials as negative as −50 mV, whereas STOCs in USMCs

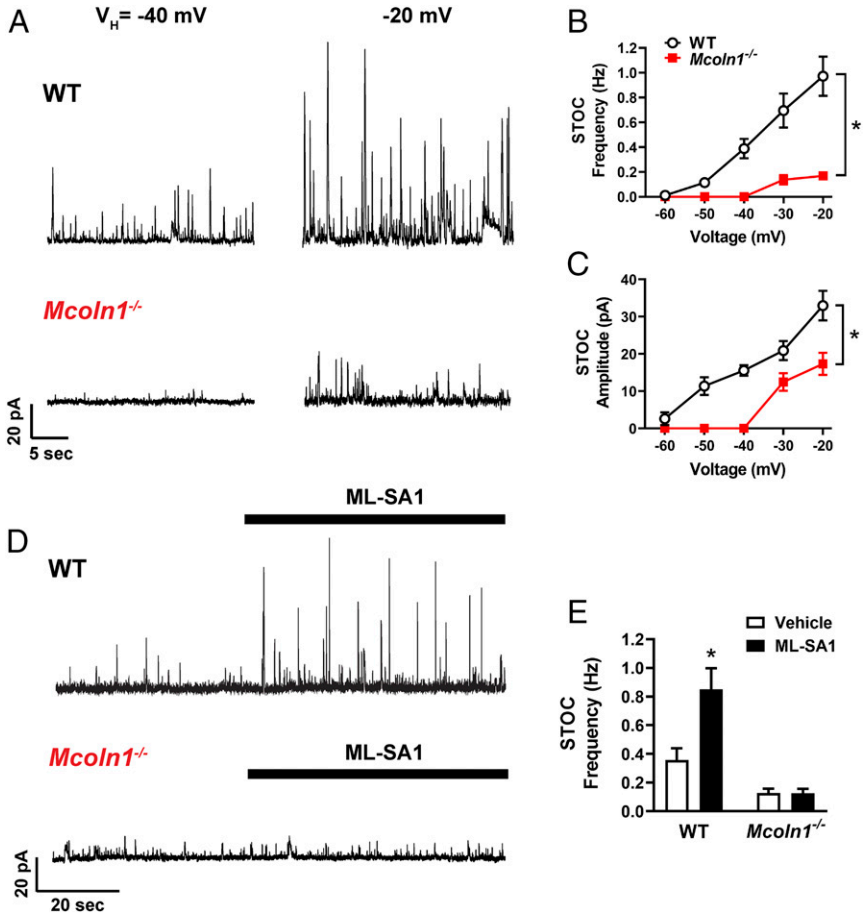

Fig. 5. Reduced spontaneous BK channel activity in BSMCs isolated from *Mcoln1*$^{-/-}$ mice. (*A*) Representative traces of STOCs recorded in the perforated-patch configuration from voltage-clamped (−40 and −20 mV) BSMCs isolated from WT and *Mcoln1*$^{-/-}$ mice. (*B* and *C*) Summary data for mean STOC frequency (*B*) and amplitude (*C*) over a range of membrane potentials (−60 to −20 mV) in BSMCs isolated from WT and *Mcoln1*$^{-/-}$ mice (WT, $n = 9$ cells from $n = 5$ mice; *Mcoln1*$^{-/-}$, $n = 7$ cells from $n = 4$ mice; $^*P < 0.05$). (*D*) Representative traces showing increases in STOC frequency following application of the TRPML activator ML-SA1 (3 μM) in BSMCs isolated from WT, but not *Mcoln1*$^{-/-}$ mice. BSMCs were voltage clamped at −30 mV. (*E*) Summary data showing the effects of ML-SA1 on STOC frequency (WT, $n = 9$ cells from $n = 5$ mice; *Mcoln1*$^{-/-}$, $n = 8$ cells from $n = 4$ mice; $^*P < 0.05$). All data are presented as means ± SEM.

from *Mcoln1*$^{-/-}$ mice were unresolved at −50 mV and reduced significantly at more positive potentials (Fig. 7*F*). Significant reductions in the frequencies and amplitudes of STOCs were observed in USMCs isolated from *Mcoln1*$^{-/-}$ mice (Fig. 7 *G* and *H*) over a range of membrane potentials (−60 to −20 mV). Taken together, these data suggest that genetic deletion of TRPML1 significantly impairs Ca^{2+} sparks and their associated STOCs in USMCs.

Sympathetic-mediated activation of proximal USM α1-ARs is the predominant contractile mechanism that prevents leakage of urine during the filling phase (44, 45). To investigate whether the hyperdistended/hypertrophic bladder phenotype observed in *Mcoln1*$^{-/-}$ mice (Fig. 1 *B* and *C*) is due to obstruction of optimal urine flow during bladder emptying as a result of proximal USM hypercontractility, we investigated USM α_1-AR responses in these mice. We found that the amplitudes of phenylephrine-induced, α_1-AR–mediated contractions of USM ring preparations from *Mcoln1*$^{-/-}$ mice were significantly larger than those in USM rings from WT mice (Fig. 7 *I* and *J*). Contractions induced by high extracellular K^+ (60 mM) did not differ between USM preparations taken from WT mice and those from *Mcoln1*$^{-/-}$ mice (*SI Appendix*, Fig. S5*B*), indicating that USM hypercontractility is most likely unrelated to any gross alterations in VDCC function or other intracellular pathways regulating USM contractility. Therefore, we demonstrate that TRPML1 channels regulate the contractility of both bladder and urethral smooth muscle, and that urethral smooth muscle hypercontractility may contribute to the distended, hypertrophic bladder phenotype observed in *Mcoln1*$^{-/-}$ mice.

***Mcoln1*$^{-/-}$ Mice Have an Overactive Bladder.** Using custom-built metabolic cages, we examined the voiding activity of size- and age-matched WT and *Mcoln1*$^{-/-}$ mice. After 2 d of acclimation, the voiding activity of mice was recorded continuously for 96 h. Parameters used to characterize voiding activity are presented as 24-h averages. *Mcoln1*$^{-/-}$ mice displayed a significant increase in voiding frequency and a decrease in the time intervals between micturition events compared with WT littermates (Fig. 8 *A*–*C*). However, the total daily urine volume voided by WT mice was significantly greater than that in *Mcoln1*$^{-/-}$ mice (Fig. 8 *D* and *E*), a finding that is not likely related to increased water consumption, as this did not differ between groups (Fig. 8*F*). These data indicate that knockout of TRPML1 leads to LUT dysfunction and OAB in *Mcoln1*$^{-/-}$ mice due to excessive constriction of bladder and urethral smooth muscle.

Discussion

The reciprocal contractile relationship of bladder and urethra smooth muscle is pivotal in maintaining normal LUT function. Here, we provide evidence that the activity of LEL-localized

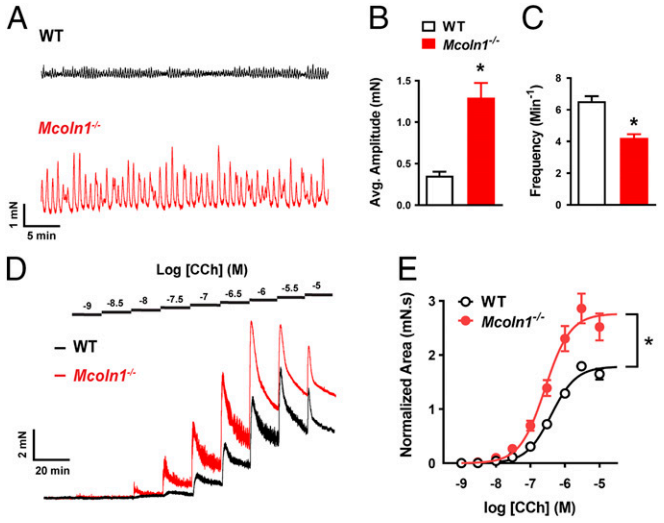

Fig. 6. BSM contractility is enhanced in *Mcoln1*$^{-/-}$ mice. (*A*) Representative isometric tension recordings showing spontaneous contractions intrinsic to WT and *Mcoln1*$^{-/-}$ BSM strips. (*B* and *C*) Summary data for mean contraction (*B*) amplitude and (*C*) frequency ($n = 11$ muscle strips from $n = 6$ animals for both groups; $^*P < 0.05$). (*D*) Representative isometric tension traces showing BSM contractions induced by the cumulative addition of increasing concentrations (1 nM to 10 μM) of the muscarinic receptor agonist CCh in WT (black) and *Mcoln1*$^{-/-}$ (red) mice. (*E*) Concentration–response data plotting the mean amplitude of CCh-induced contractions of BSM strips from WT and *Mcoln1*$^{-/-}$ mice, normalized to the high-K^+ response (WT, $n = 8$ muscle strips from $n = 4$ mice; *Mcoln1*$^{-/-}$, $n = 9$ muscle strips from $n = 5$ mice; $^*P < 0.05$). All data are presented as means ± SEM.

TRPML1 channels provides negative feedback that regulates LUT SMC excitability and contractility. Using live-cell 4D imaging and superresolution microscopy, we found that the vast majority of LELs were nearly immobile in native BSMCs, thereby permitting the formation of stable signaling complexes between TRPML1 channels and RyR2s. Our findings also indicated that TRPML1 channels are essential for activation of the Ca^{2+} spark–BK channel pathway. Genetic ablation of TRPML1 channels led to bladder and urethra smooth muscle hypercontractility, resulting in the development of bladder outlet obstruction and symptoms of OAB. Thus, we conclude that TRPML1 channels are critical for the generation of RyR2-mediated Ca^{2+} sparks in SMCs, regulation of LUT smooth muscle contractility, and normal micturition.

The Ca^{2+} spark–BK channel signaling pathway regulates BSM excitability (29). BK channels provide negative feedback that limits and controls the amplitude and duration of spontaneous action potentials and associated nonvoiding contractions (22, 46, 47). Mice lacking the BK channel pore-forming α-subunit (48, 49) and heterozygous RyR2-knockout mice (27) show absent or decreased STOCs, enhanced amplitude of spontaneous contractions, and increased urination frequency. Under pathophysiological conditions, spontaneous contractions are increased in patients with OAB (50, 51), a finding that has been linked to reduced bladder BKα expression (52) and highlighting the importance of the Ca^{2+} spark–BK channel signaling pathway in regulating bladder excitability during filling. Data from the current study show that TRPML1 channels are necessary for the generation of Ca^{2+} sparks and their associated STOC activity, because these events were greatly reduced or absent from BSMCs lacking TRPML1. Consistent with this observation, knockout of TRPML1 led to enhanced BSM spontaneous contractions and increased urination frequency, indicative of OAB. Thus, our results identify TRPML1 channels as a component of the Ca^{2+} spark–BK signaling cascade in BSMCs.

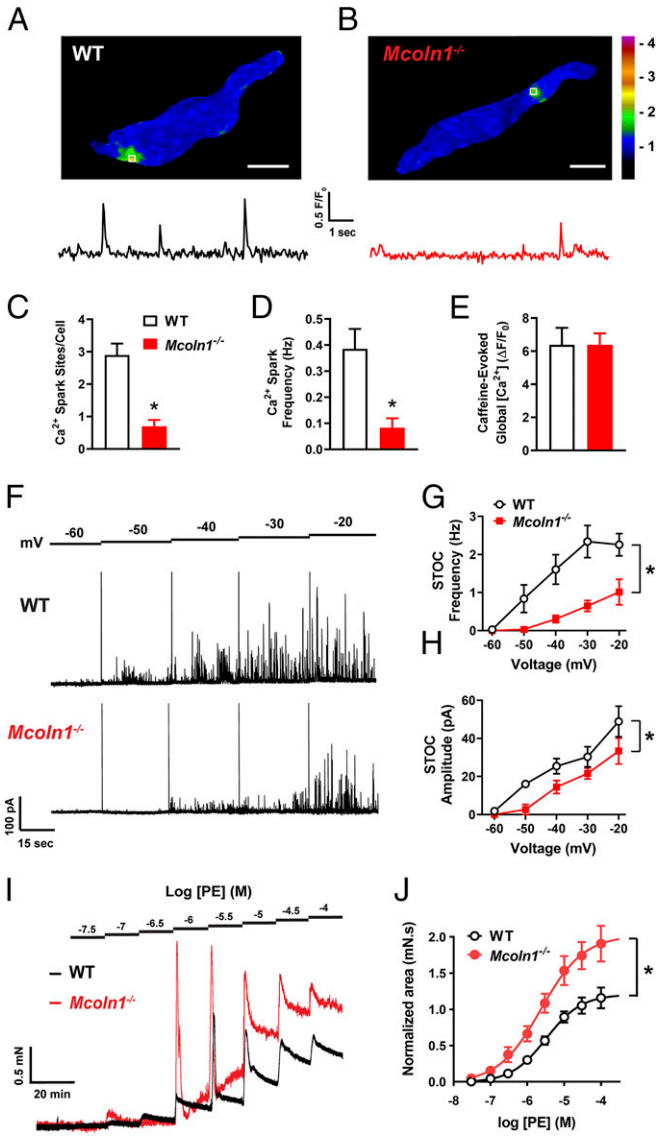

Fig. 7. USMCs from *Mcoln1*$^{-/-}$ mice show impaired Ca^{2+} sparks and STOC activity, leading to USM hypercontractility. (*A*) Representative confocal image of a Ca^{2+} spark site (Scale bar, 10 μm.) in a Fluo-4 AM loaded USMC from a WT mouse, and trace showing changes in fractional fluorescence (F/F_0) in a defined region of interest (white box). (*B*) Representative confocal image (Scale bar, 10 μm.) and complimentary trace recorded from a USMC isolated from a *Mcoln1*$^{-/-}$ mouse showing reduced Ca^{2+} spark activity. (*C* and *D*) Summary data showing (*C*) the number of spontaneous Ca^{2+} spark sites per cell and (*D*) Ca^{2+} spark frequency in USMCs isolated from WT and *Mcoln1*$^{-/-}$ mice (WT, $n = 19$ cells from $n = 4$ mice; *Mcoln1*$^{-/-}$, $n = 20$ cells from $n = 4$ mice; $^*P < 0.05$). (*E*) Total SR Ca^{2+} store load in USMCs from WT and *Mcoln1*$^{-/-}$ mice, assessed by imaging changes in global intracellular $[Ca^{2+}]$ in response to administration of caffeine (10 mM) (WT, $n = 7$ cells from $n = 4$ mice; *Mcoln1*$^{-/-}$, $n = 8$ cells from $n = 4$ mice). (*F*) Representative traces of STOCs recorded in the perforated-patch configuration from voltage-clamped (−60 to −20 mV) USMCs isolated from WT and *Mcoln1*$^{-/-}$ mice. (*G* and *H*) Summary data for mean STOC frequency (*G*) and amplitude (*H*) over a range of membrane potentials (−60 to −20 mV) in WT and *Mcoln1*$^{-/-}$ mice ($n = 6$ cells from $n = 4$ mice in both groups; $^*P < 0.05$). (*I*) Representative isometric tension traces showing USM contractions induced by the cumulative addition of increasing concentrations (30 nM to 100 μM) of the α1-AR agonist phenylephrine (PE) in WT (black) and *Mcoln1*$^{-/-}$ (red) mice. (*J*) Concentration–response data plotting mean amplitudes of PE-induced contractions of USM ring preparations from WT and *Mcoln1*$^{-/-}$ mice, normalized to the high-K^+ response (WT, $n = 6$ from $n = 6$ mice; *Mcoln1*$^{-/-}$, $n = 6$ from $n = 6$ mice; $^*P < 0.05$). All data are presented as means ± SEM.

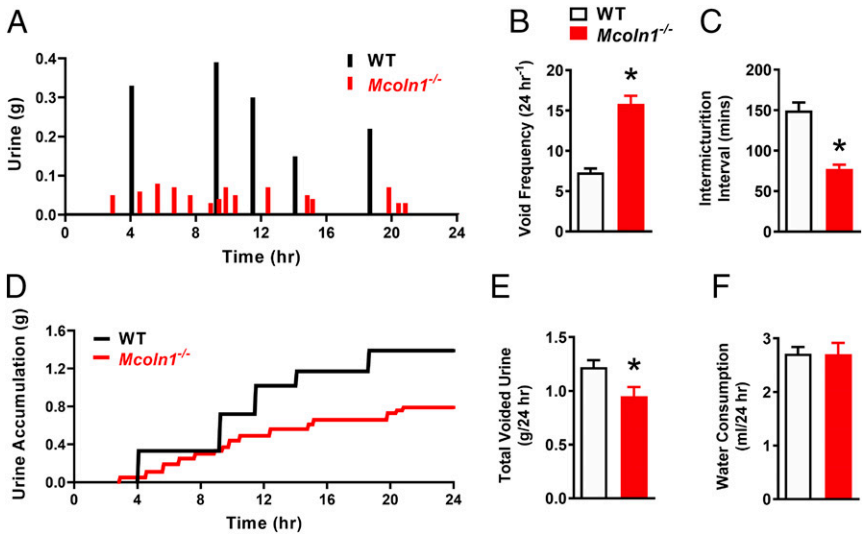

Fig. 8. *Mcoln1*$^{-/-}$ mice show hyperactive voiding. (*A*) Representative voiding micturogram displaying the micturition activity of WT (black) and *Mcoln1*$^{-/-}$ (red) mice over a 24-h period. (*B* and *C*) Summary data showing the daily average void frequency (*B*) and intermicturition interval (*C*) for WT and *Mcoln1*$^{-/-}$ mice (WT, $n = 6$; *Mcoln1*$^{-/-}$, $n = 6$; $^*P < 0.05$). (*D*) Representative trace, complimentary to the micturogram in *A*, showing urine accumulation in WT (black) and *Mcoln1*$^{-/-}$ (red) mice. (*E* and *F*) Summary data showing the total daily voided urine volume (*E*) and water consumption (*F*) for WT and *Mcoln1*$^{-/-}$ mice (WT, $n = 6$; *Mcoln1*$^{-/-}$, $n = 6$; $^*P < 0.05$). All data are presented as means ± SEM.

Where do TRPML1 channels fit in the canonical Ca^{2+} spark–BK signaling pathway? We propose a model based on the nanoscale localization of TRPML1 channels with RyR2s in SMCs. In mammalian cells, the subcellular localization of TRPML1 channels is limited to the membranes of LELs. A significant finding in the current study is that LELs are essentially immobile in native BSMCs, a result that contrasts sharply with the high levels of LEL mobility we observed in proliferative BSMCs and that others have reported in many other cell types (53). Furthermore, superresolution analyses of native BSMCs revealed that a large number of RyR2 clusters are located within 40 nm or less of TRPML1 clusters expressed on LELs. The steepness of the gradient between LEL intraluminal [Ca^{2+}] (~0.5 mM) (30) and the surrounding cytosol (100 nM) leads us to propose that the opening of Ca^{2+}-permeable TRPML channel clusters on the membrane of LELs activates nearby RyR2 through a Ca^{2+}-induced Ca^{2+} release mechanism, triggering Ca^{2+} sparks and downstream BK channel-mediated STOCs. Replenishment of intraluminal LEL Ca^{2+} is required for sustained operation of this signaling complex. This process is not fully understood, but an unidentified H^+/Ca^{2+} exchanger has been suggested as a plausible candidate (30).

Although it has been widely and convincingly shown that the force of BSM spontaneous contractions is enhanced upon inhibition of the Ca^{2+} spark–BK channel signaling pathway, the effect of suppressing this pathway on spontaneous contraction frequency appears to vary between species. For example, contractility experiments have shown that pharmacological blockade of BK channels increases contraction frequency in BSM from guinea pigs (54) and humans (55), but reduces it in mice (46, 56). Our data show that the amplitudes of BSM spontaneous contractions are significantly increased in *Mcoln1*$^{-/-}$ mice in association with a decrease in contraction frequency, a result consistent with the literature on murine BSM (46, 56). Extrapolating from these disparities to a mechanism is difficult; however, one simple explanation could be that the decreased contraction frequency observed in mice upon inhibition of the Ca^{2+} spark–BK channel signaling pathway is caused by prolonged membrane depolarization and increased cytosolic [Ca^{2+}] during a single spontaneous contraction, leading to a longer than normal quiescent period due to voltage or Ca^{2+} inactivation of VDCCs.

Voiding contractions of the bladder are cholinergic in origin and are predominantly mediated by M_3Rs. These responses involve VDCC-mediated Ca^{2+} influx and IP_3-mediated Ca^{2+} release from the SR of BSMCs (42). M_3R-mediated contractions of BSM are enhanced by both genetic deletion (49) and pharmacological inhibition (56, 57) of BK channels. In the current study, CCh-induced contractions of BSM strips from *Mcoln1*$^{-/-}$ mice were greatly increased compared with those from WT mice. Because application of CCh significantly inhibits STOC activity and depletes SR Ca^{2+} via IP_3-mediated store release (58), the contribution of Ca^{2+} spark–BK channel signaling to M_3R-mediated responses in BSMCs is likely minimal. The Ca^{2+} spark–BK channel signaling pathway is essential for mediating resting membrane potential in BSMCs. For example, the resting membrane potential of BSMCs isolated from BKα-null mice (−25.8 mV) is significantly depolarized compared with that of BSMCs from WT mice (−45.5 mV) (59). Our data show that TRPML1 channels are critical in regulating Ca^{2+} spark–BK channel signaling. Therefore, the expectation is that genetic deletion of TRPML1 would depolarize BSMCs, leading to a more forceful contraction upon M_3R stimulation, providing a likely explanation for the hypercontractility of BSM in response to M_3R activation in *Mcoln1*$^{-/-}$ mice.

Bladder outlet obstruction (BOO) is a LUT disorder in which urine outflow is restricted, most commonly by benign prostatic hyperplasia (BPH) and/or increased α-adrenergic activity/expression in the bladder neck and prostatic urethra. BOO is accompanied by bladder hypertrophy and remodeling, which serves to compensate for the increased resistance to flow (60). Both overactive and underactive voiding activity have been observed in rodent models of BOO (61). Schroder et al. (62) reported that conscious mice with moderate urethral obstruction displayed two types of micturition characteristics: 1) increased frequency, hyperactive nonvoiding contractions, reduced voiding volumes, and low bladder capacity; and 2) reduced micturition frequency, a slight increase in nonvoiding contractions, normal voiding volumes, increased bladder capacity with hypertrophy, and residual urine. In the current study, *Mcoln1*$^{-/-}$ mice displayed hyperdistended

bladders with hypertrophy reminiscent of BOO-induced underactivity (62). Because α_1-AR responses were significantly enhanced in *Mcoln1*$^{-/-}$ mice, this phenotype is most likely brought about by the reduction in urine outflow due to proximal USM hypercontractility. However, *Mcoln1*$^{-/-}$ mice showed a drastic increase in voiding frequency compared with WT mice, and BSM from *Mcoln1*$^{-/-}$ mice exhibited hyperactive spontaneous contractions indicative of bladder overactivity. Therefore, it appears from our data that knockout of TRPML1 renders the proximal USM hypercontractile, giving rise to BOO-induced bladder distension and hypertrophy. The typical signs of bladder underactivity associated with this pathology are overpowered by the lack of TRPML1-mediated regulation of the Ca^{2+}spark–BK channel signaling pathway in *Mcoln1*$^{-/-}$ mice, leading to BSM hypercontractility and symptoms of OAB together with bladder distension and hypertrophy. Decreased expression of BKα has been reported in patients with BPH-induced BOO (63) and in rodent models of BOO (64). However, this is not likely a contributing factor to bladder hyperactivity in the current study since expression levels of BKα and BKβ1 did not differ significantly between bladders from WT and *Mcoln1*$^{-/-}$ mice.

During the filling phase, USM develops spontaneous tone; this is further enhanced by sympathetic neurotransmission to produce a urethral closure pressure that exceeds intravesical bladder pressure, thus maintaining continence (44). The role of BK channels in regulating these USM mechanisms (65) has not been studied as extensively as those in the bladder (66), probably reflecting difficulties in obtaining sufficient urethral tissue from small rodents such as mice. Patch-clamp recordings of rabbit USMCs show that these cells possess large voltage-evoked BK currents that are mediated by Ca^{2+} release via RyRs (31). Spontaneous hyperpolarizations in pig USMCs are dependent on BK channels (23), and the amplitude and duration of pulse-evoked action potentials, as well as urethra contractility, are significantly increased upon BK channel inhibition (43). While in situ imaging of USMCs in intact rabbit (67) and mouse (68) urethral muscle preparations has demonstrated propagating intracellular Ca^{2+} waves, the optical detection of Ca^{2+} sparks has not been reported in these cells, despite reports that STOCs are present,and is mediated by SR Ca^{2+} in isolated rabbit USMCs (31). The current study demonstrates the presence of Ca^{2+} sparks in isolated USMCs, and that these events are mediated by RyRs. We found that USMCs display on average three Ca^{2+} spark sites per cell at a mean spark frequency of ∼0.4 Hz. Both Ca^{2+} sparks and STOC activity were significantly impaired in USMCs isolated from *Mcoln1*$^{-/-}$ mice, and USM tissue strips from these mice were hypercontractile. Surprisingly, the canonical pathway of BK channel-mediated regulation of VDCC activity is not as clear in USMCs, and there appears to be significant species differences. For example, robust L-type Ca^{2+} currents are detected in rabbit (69) and human (70) USMCs. Upon VDCC channel inhibition, spontaneous action potentials in rabbit USMCs are reduced (71), USM tone in pigs is abolished (72), and α_1-AR–mediated contractions of rat USM are greatly impaired (73). In contrast, it has been shown that α_1-AR–mediated Ca^{2+} responses and contractions of mouse USM are resistant to VDCC inhibition and appear to be reliant instead on store-operated Ca^{2+} entry (68). Our study showed that genetic deletion of TRPML1 impairs Ca^{2+} sparks and their associated BK channel activity in isolated murine USMCs and thereby enhances urethral contractility. However, considering the paucity of previous investigations into the role of the Ca^{2+} spark–BK channel pathway and varying reports on species differences in VDCC function, it is difficult to accurately determine the subcellular mechanisms by which TRPML1 influences urethral contractility.

The Ca^{2+} spark–BK channel signaling pathway is a critical regulator of SMC excitability (24). Our study demonstrates that TRPML1 channels are essential for this pathway in bladder SMCs, showing that they act upstream of RyR2s to cause generation of Ca^{2+} sparks and subsequent activation of plasma membrane BK channels. In urethra SMCs, TRPML1 regulates Ca^{2+} sparks, STOC activity, and muscle contractility. Although, the manner in which TRPML1 influences these pathways is less obvious, our findings collectively support the conclusion that TRPML1 is critical for the regulation of LUT smooth muscle contractility.

Materials and Methods

See *SI Appendix, SI Materials and Methods* for a more detailed description of experimental protocols.

Animals, Tissue Preparation, and Isolation of SMCs. Adult (16 to 20 wk) male WT C57BL/6J mice, homozygous global *Mcoln1*$^{-/-}$ mice, and *smMHC*$^{Cre/eGFP}$ transgenic reporter mice were used in this study. The urinary tract was removed from humanely killed mice and placed in ice-cold Krebs solution. Both the proximal urethra and urinary bladder smooth muscle were dissected from mice, removing any excess fat and connective tissue. SMCs were isolated by placing small pieces (0.25 mm^3) of BSM or proximal USM into Ca^{2+}-free physiological saline solution (PSS) containing papain, dithioerythritol, and bovine serum albumin (BSA) at 37 °C for 25 min, then into Ca^{2+}-free PSS containing type II collagenase, BSA, and 100 μM $CaCl_2$ at 37 °C for 6 to 7 min. Single SMCs were liberated by gentle trituration.

Molecular Biology. RNA was extracted from BSM strips using homogenization in TRIzol reagent, then subsequently purified and reversed transcribed into cDNA using qScript cDNA Supermix. ddPCR was performed using QX200 ddPCR EvaGreen Supermix, custom-designed primers (*SI Appendix*, Table S1), and cDNA templates. Generated droplet emulsions were amplified using a C1000 Touch Thermal Cycler and fluorescence intensity of individual droplets was measured with the QX200 Droplet Reader. qRT-PCR was performed on a QuantStudio 3 system using Fast SYBR Green Master Mix.

Protein Extraction and Westerns. Proteins from BSM strips were extracted by homogenization in radioimmunoprecipitation assay buffer and protease inhibitor mixture. TRPML1 protein expression was detected using an anti-TRPML1 antibody, horseradish peroxidase-conjugated secondary antibodies, and luminol-peroxide mix. Proteins were resolved and fluorescence intensity was measured using a Wes automated capillary-based protein-detection system.

LEL Visualization and Tracking. LELs were visualized by labeling freshly isolated and cultured BSMCs with LysoTracker Red. Four-dimensional imaging of BSMCs was performed using a lattice light-sheet microscope (LLSM) (33). Briefly, BSMCs were adhered to round coverslips (5 mm), mounted to a sample holder, and placed into the LLSM bath immersed in Ca^{2+}-containing PSS. Imaging was conducted with dithered mode set to 20-ms exposures. Z-steps (80 to 120) were collected with a 0.4-μm step size. Transformed recordings were subsequently analyzed using the 4D particle tracking function of IMARIS software.

GSDIM Superresolution Microscopy. Seeded BSMCs were fixed in 2% paraformaldehyde, permeabilized with 0.1% Triton X, and blocked with 50% SEA Block solution in phosphate-buffered saline. Immunolabeling was performed using primary antibodies against Lamp-1, RyR2, and/or TRPML1. Detection was performed using Alexa Fluor 568- or 647-conjugated secondary antibodies. Coverslips were mounted to slides in a thiol-based photo-switching imaging buffer, and superresolution images were acquired using a GSDIM imaging system (Leica). Postacquisition image analyses of cluster size distribution were performed using binary masks of the images in ImageJ software.

Ca^{2+} Sparks. SMCs were loaded with the Ca^{2+}-sensitive fluorophore Fluo-4 AM (1 μM) for 20 min at room temperature then washed and stored in Ca^{2+}-containing PSS. Images were acquired using an iXon 897 electron multiplying charge-coupled device camera and a 100× oil-immersion objective at 33 frames per second (fps).

Patch-Clamp Electrophysiology. All currents from SMCs were recorded at room temperature (22 °C) in Ca^{2+} containing PSS using an AxoPatch 200B amplifier and pClamp software. Perforated-patch (amphotericin B; 250 μg/mL) or conventional whole-cell configurations were used to record STOCs and whole-cell K^+ currents, respectively.

Isometric Tension Recordings. BSM strips and proximal USM ring preparations were attached to a tissue holder, immersed in heated (37 °C) water-jacketed organ baths containing Krebs solution, and bubbled with 95% O_2/5% CO_2. Force contraction data were acquired using AcqKnowledge software and analyzed using pClamp 11 software.

Voiding Activity Analysis. The voiding activity of freely moving, conscious WT and *Mcoln1*$^{-/-}$ mice was recorded over a 96-h period, using custom-built metabolic cages. Parameters measuring voiding activity are presented as daily (24 h) averages.

Statistical Analysis. All data are presented as means ± SEM. Values of "*n*" refer to the number of individual experiments. A *P* value of <0.05 was considered to be statistically significant for all analyses.

Data Availability. All data needed to evaluate the conclusions in the paper are present in the paper and *SI Appendix*.

ACKNOWLEDGMENTS. We thank Dr. Caroline Cobine for providing the use of her isometric tension equipment, Dr. Sang Dong Koh for providing the use of his custom voiding activity cages, and Dr. Adrian Bonev (University of Vermont) for providing SparkAn software for the analysis of Ca^{2+} sparks. This study was supported by grants from the NIH (National, Heart, Lung, and Blood Institute R01HL091905, R01HL137852, R01HL139585, R01146054, and R01HL122770; National Institute of Neurological Disorders and Stroke RF1NS110044 and R61NS115132; and National Institute of General Medical Sciences [NIGMS] P20GM130459 [to S.E.] and P30GM110767 and R01DK119491 [to K.M.S.]). The FACS/Flow Cytometry Shared Resource Laboratory Core at the University of Nevada, Reno School of Medicine is supported by grants from the NIH (P01DK041315 and P30GM110767). The Transgenic Genotyping and Phenotyping Core at the COBRE Center for Molecular and Cellular Signaling in the Cardiovascular System, University of Nevada, Reno, is maintained by a grant from NIH/NIGMS (P20GM130459 Sub#5451), as is the High Spatial and Temporal Resolution Imaging Core at the COBRE Center for Molecular and Cellular Signaling in the Cardiovascular System, University of Nevada, Reno (P20GM130459 Sub#5452).

1. C. Montell, The TRP superfamily of cation channels. *Sci. STKE* **2005**, re3 (2005).
2. M. Sun *et al*., Mucolipidosis type IV is caused by mutations in a gene encoding a novel transient receptor potential channel. *Hum. Mol. Genet.* **9**, 2471–2478 (2000).
3. K. Venkatachalam, C. O. Wong, M. X. Zhu, The role of TRPMLs in endolysosomal trafficking and function. *Cell Calcium* **58**, 48–56 (2015).
4. J. M. Lindvall, K. E. Blomberg, A. Wennborg, C. I. Smith, Differential expression and molecular characterisation of Lmo7, Myo1e, Sash1, and Mcoln2 genes in Btk-defective B-cells. *Cell. Immunol.* **235**, 46–55 (2005).
5. M. A. Samie *et al*., The tissue-specific expression of TRPML2 (MCOLN-2) gene is influenced by the presence of TRPML1. *Pflugers Arch.* **459**, 79–91 (2009).
6. H. Xu, M. Delling, L. Li, X. Dong, D. E. Clapham, Activating mutation in a mucolipin transient receptor potential channel leads to melanocyte loss in varitint-waddler mice. *Proc. Natl. Acad. Sci. U.S.A.* **104**, 18321–18326 (2007).
7. R. Bargal *et al*., Identification of the gene causing mucolipidosis type IV. *Nat. Genet.* **26**, 118–123 (2000).
8. X. P. Dong *et al*., PI(3,5)P(2) controls membrane trafficking by direct activation of mucolipin Ca(2+) release channels in the endolysosome. *Nat. Commun.* **1**, 38 (2010).
9. X. P. Dong *et al*., The type IV mucolipidosis-associated protein TRPML1 is an endolysosomal iron release channel. *Nature* **455**, 992–996 (2008).
10. X. Cheng, D. Shen, M. Samie, H. Xu, Mucolipins: Intracellular TRPML1-3 channels. *FEBS Lett.* **584**, 2013–2021 (2010).
11. S. Vergarajauregui, P. S. Connelly, M. P. Daniels, R. Puertollano, Autophagic dysfunction in mucolipidosis type IV patients. *Hum. Mol. Genet.* **17**, 2723–2737 (2008).
12. X. Zhang *et al*., MCOLN1 is a ROS sensor in lysosomes that regulates autophagy. *Nat. Commun.* **7**, 12109 (2016).
13. K. Venkatachalam *et al*., Motor deficit in a Drosophila model of mucolipidosis type IV due to defective clearance of apoptotic cells. *Cell* **135**, 838–851 (2008).
14. B. Venugopal *et al*., Neurologic, gastric, and opthalmologic pathologies in a murine model of mucolipidosis type IV. *Am. J. Hum. Genet.* **81**, 1070–1083 (2007).
15. A. F. Brading, The physiology of the mammalian urinary outflow tract. *Exp. Physiol.* **84**, 215–221 (1999).
16. D. P. Keane, S. O'Sullivan, Urinary incontinence: Anatomy, physiology and pathophysiology. *Best Pract. Res. Clin. Obstet. Gynaecol.* **14**, 207–226 (2000).
17. T. J. Heppner, N. R. Tykocki, D. Hill-Eubanks, M. T. Nelson, Transient contractions of urinary bladder smooth muscle are drivers of afferent nerve activity during filling. *J. Gen. Physiol.* **147**, 323–335 (2016).
18. M. J. Drake *et al*., What are the origins and relevance of spontaneous bladder contractions? ICI-RS 2017. *Neurourol. Urodyn.* **37**, S13–S19 (2018).
19. C. J. Fowler, D. Griffiths, W. C. de Groat, The neural control of micturition. *Nat. Rev. Neurosci.* **9**, 453–466 (2008).
20. P. Abrams *et al*.; Standardisation Sub-Committee of the International Continence Society, The standardisation of terminology in lower urinary tract function: Report from the standardisation sub-committee of the international continence society. *Urology* **61**, 37–49 (2003).
21. H. Hashitani, A. F. Brading, H. Suzuki, Correlation between spontaneous electrical, calcium and mechanical activity in detrusor smooth muscle of the Guinea-pig bladder. *Br. J. Pharmacol.* **141**, 183–193 (2004).
22. H. Hashitani, A. F. Brading, Ionic basis for the regulation of spontaneous excitation in detrusor smooth muscle cells of the Guinea-pig urinary bladder. *Br. J. Pharmacol.* **140**, 159–169 (2003).
23. A. F. Brading, Spontaneous activity of lower urinary tract smooth muscles: Correlation between ion channels and tissue function. *J. Physiol.* **570**, 13–22 (2006).
24. J. H. Jaggar, V. A. Porter, W. J. Lederer, M. T. Nelson, Calcium sparks in smooth muscle. *Am. J. Physiol. Cell Physiol.* **278**, C235–C256 (2000).
25. G. M. Herrera, T. J. Heppner, M. T. Nelson, Voltage dependence of the coupling of Ca(2+) sparks to BK(Ca) channels in urinary bladder smooth muscle. *Am. J. Physiol. Cell Physiol.* **280**, C481–C490 (2001).
26. Y. Ohi *et al*., Local Ca(2+) transients and distribution of BK channels and ryanodine receptors in smooth muscle cells of Guinea-pig vas deferens and urinary bladder. *J. Physiol.* **534**, 313–326 (2001).
27. S. Hotta *et al*., Ryanodine receptor type 2 deficiency changes excitation-contraction coupling and membrane potential in urinary bladder smooth muscle. *J. Physiol.* **582**, 489–506 (2007).
28. G. Ji *et al*., RYR2 proteins contribute to the formation of Ca(2+) sparks in smooth muscle. *J. Gen. Physiol.* **123**, 377–386 (2004).
29. G. V. Petkov, Central role of the BK channel in urinary bladder smooth muscle physiology and pathophysiology. *Am. J. Physiol. Regul. Integr. Comp. Physiol.* **307**, R571–R584 (2014).
30. K. A. Christensen, J. T. Myers, J. A. Swanson, pH-dependent regulation of lysosomal calcium in macrophages. *J. Cell Sci.* **115**, 599–607 (2002).
31. B. D. Kyle *et al*., Mechanisms underlying activation of transient BK current in rabbit urethral smooth muscle cells and its modulation by IP3-generating agonists. *Am. J. Physiol. Cell Physiol.* **305**, C609–C622 (2013).
32. G. Griffiths, B. Hoflack, K. Simons, I. Mellman, S. Kornfeld, The mannose 6-phosphate receptor and the biogenesis of lysosomes. *Cell* **52**, 329–341 (1988).
33. B. C. Chen *et al*., Lattice light-sheet microscopy: Imaging molecules to embryos at high spatiotemporal resolution. *Science* **346**, 1257998 (2014).
34. J. Bierwagen *et al*., Far-field autofluorescence nanoscopy. *Nano Lett.* **10**, 4249–4252 (2010).
35. J. Fölling *et al*., Fluorescence nanoscopy by ground-state depletion and single-molecule return. *Nat. Methods* **5**, 943–945 (2008).
36. I. Testa *et al*., Multicolor fluorescence nanoscopy in fixed and living cells by exciting conventional fluorophores with a single wavelength. *Biophys. J.* **99**, 2686–2694 (2010).
37. H. A. T. Pritchard *et al*., Nanoscale coupling of junctophilin-2 and ryanodine receptors regulates vascular smooth muscle cell contractility. *Proc. Natl. Acad. Sci. U.S.A.* **116**, 21874–21881 (2019).
38. H. A. T. Pritchard, P. W. Pires, E. Yamasaki, P. Thakore, S. Earley, Nanoscale remodeling of ryanodine receptor cluster size underlies cerebral microvascular dysfunction in Duchenne muscular dystrophy. *Proc. Natl. Acad. Sci. U.S.A.* **115**, E9745–E9752 (2018).
39. P. Thakore *et al*., TRPML1 channels initiate Ca^{2+} sparks in vascular smooth muscle cells. *Sci. Signal.* **13**, eaba1015 (2020).
40. D. Bandyopadhyay, A. Cyphersmith, J. A. Zapata, Y. J. Kim, C. K. Payne, Lysosome transport as a function of lysosome diameter. *PLoS One* **9**, e86847 (2014).
41. D. Shen *et al*., Lipid storage disorders block lysosomal trafficking by inhibiting a TRP channel and lysosomal calcium release. *Nat. Commun.* **3**, 731 (2012).
42. E. P. Frazier, S. L. Peters, A. S. Braverman, M. R. Ruggieri Sr, M. C. Michel, Signal transduction underlying the control of urinary bladder smooth muscle tone by muscarinic receptors and beta-adrenoceptors. *Naunyn Schmiedebergs Arch. Pharmacol.* **377**, 449–462 (2008).
43. B. Kyle *et al*., Contribution of Kv2.1 channels to the delayed rectifier current in freshly dispersed smooth muscle cells from rabbit urethra. *Am. J. Physiol. Cell Physiol.* **301**, C1186–C1200 (2011).
44. K. E. Andersson, A. J. Wein, Pharmacology of the lower urinary tract: Basis for current and future treatments of urinary incontinence. *Pharmacol. Rev.* **56**, 581–631 (2004).
45. W. G. Hill, Control of urinary drainage and voiding. *Clin. J. Am. Soc. Nephrol.* **10**, 480–492 (2015).
46. G. M. Herrera, T. J. Heppner, M. T. Nelson, Regulation of urinary bladder smooth muscle contractions by ryanodine receptors and BK and SK channels. *Am. J. Physiol. Regul. Integr. Comp. Physiol.* **279**, R60–R68 (2000).
47. T. J. Heppner, A. D. Bonev, M. T. Nelson, Ca(2+)-activated K+ channels regulate action potential repolarization in urinary bladder smooth muscle. *Am. J. Physiol.* **273**, C110–C117 (1997).
48. A. L. Meredith, K. S. Thorneloe, M. E. Werner, M. T. Nelson, R. W. Aldrich, Overactive bladder and incontinence in the absence of the BK large conductance Ca2+-activated K+ channel. *J. Biol. Chem.* **279**, 36746–36752 (2004).
49. K. S. Thorneloe, A. L. Meredith, A. M. Knorn, R. W. Aldrich, M. T. Nelson, Urodynamic properties and neurotransmitter dependence of urinary bladder contractility in the BK channel deletion model of overactive bladder. *Am. J. Physiol. Renal Physiol.* **289**, F604–F610 (2005).
50. A. F. Brading, A myogenic basis for the overactive bladder. *Urology* **50**, 57–67, discussion 68-73 (1997).
51. S. Oger *et al*., Effects of potassium channel modulators on myogenic spontaneous phasic contractile activity in human detrusor from neurogenic patients. *BJU Int.* **108**, 604–611 (2011).

52. K. L. Hristov *et al*., Neurogenic detrusor overactivity is associated with decreased expression and function of the large conductance voltage- and Ca(2+)-activated K(+) channels. *PLoS One* **8**, e68052 (2013).
53. X. Li *et al*., A molecular mechanism to regulate lysosome motility for lysosome positioning and tubulation. *Nat. Cell Biol.* **18**, 404–417 (2016).
54. T. Imai *et al*., Effects of different types of K+ channel modulators on the spontaneous myogenic contraction of Guinea-pig urinary bladder smooth muscle. *Acta Physiol. Scand.* **173**, 323–333 (2001).
55. W. Xin, Q. Cheng, R. P. Soder, E. S. Rovner, G. V. Petkov, Constitutively active phosphodiesterase activity regulates urinary bladder smooth muscle function: Critical role of KCa1.1 channel. *Am. J. Physiol. Renal Physiol.* **303**, F1300–F1306 (2012).
56. G. V. Petkov *et al*., Beta1-subunit of the Ca2+-activated K+ channel regulates contractile activity of mouse urinary bladder smooth muscle. *J. Physiol.* **537**, 443–452 (2001).
57. H. Cernecka *et al*., β3-Adrenoceptor-mediated relaxation of rat and human urinary bladder: Roles of BKCa channels and Rho kinase. *Naunyn Schmiedebergs Arch. Pharmacol.* **388**, 749–759 (2015).
58. S. P. Parajuli, G. V. Petkov, Activation of muscarinic M3 receptors inhibits large-conductance voltage- and Ca2+-activated K+ channels in rat urinary bladder smooth muscle cells. *Am. J. Physiol. Cell Physiol.* **305**, C207–C214 (2013).
59. F. Sprossmann *et al*., Inducible knockout mutagenesis reveals compensatory mechanisms elicited by constitutive BK channel deficiency in overactive murine bladder. *FEBS J.* **276**, 1680–1697 (2009).
60. K. E. Andersson, Storage and voiding symptoms: Pathophysiologic aspects. *Urology* **62**, 3–10 (2003).
61. K. E. Andersson, R. Soler, C. Füllhase, Rodent models for urodynamic investigation. *Neurourol. Urodyn.* **30**, 636–646 (2011).
62. A. Schröder, B. Uvelius, D. Newgreen, K. E. Andersson, Bladder overactivity in mice after 1 week of outlet obstruction. Mainly afferent dysfunction? *J. Urol.* **170**, 1017–1021 (2003).
63. S. Chang *et al*., Detrusor overactivity is associated with downregulation of large-conductance calcium- and voltage-activated potassium channel protein. *Am. J. Physiol. Renal Physiol.* **298**, F1416–F1423 (2010).
64. M. Aydin *et al*., Large-conductance calcium-activated potassium channel activity, as determined by whole-cell patch clamp recording, is decreased in urinary bladder smooth muscle cells from male rats with partial urethral obstruction. *BJU Int.* **110**, E402–E408 (2012).
65. B. D. Kyle, Ion channels of the mammalian urethra. *Channels (Austin)* **8**, 393–401 (2014).
66. G. V. Petkov, Role of potassium ion channels in detrusor smooth muscle function and dysfunction. *Nat. Rev. Urol.* **9**, 30–40 (2011).
67. H. Hashitani, H. Suzuki, Properties of spontaneous Ca2+ transients recorded from interstitial cells of Cajal-like cells of the rabbit urethra in situ. *J. Physiol.* **583**, 505–519 (2007).
68. B. T. Drumm *et al*., Ca^{2+} signalling in mouse urethral smooth muscle in situ: Role of Ca^{2+} stores and Ca^{2+} influx mechanisms. *J. Physiol.* **596**, 1433–1466 (2018).
69. G. P. Sergeant, M. A. Hollywood, K. D. McCloskey, K. D. Thornbury, N. G. McHale, Specialised pacemaking cells in the rabbit urethra. *J. Physiol.* **526**, 359–366 (2000).
70. M. A. Hollywood *et al*., T- and L-type Ca2+ currents in freshly dispersed smooth muscle cells from the human proximal urethra. *J. Physiol.* **550**, 753–764 (2003).
71. H. Hashitani, Y. Yanai, K. Kohri, H. Suzuki, Heterogeneous CPA sensitivity of spontaneous excitation in smooth muscle of the rabbit urethra. *Br. J. Pharmacol.* **148**, 340–349 (2006).
72. J. E. Greenland, N. Dass, A. F. Brading, Intrinsic urethral closure mechanisms in the female pig. *Scand. J. Urol. Nephrol. Suppl.* **179**, 75–80 (1996).
73. R. Chess-Williams, N. Aston, C. Couldwell, Alpha 1A-adrenoceptor subtype mediates contraction of the rat urethra. *J. Auton. Pharmacol.* **14**, 375–381 (1994).